metals

MDPI

Article

Cobalt Oxide-Decorated on Carbon Derived from Onion Skin Biomass for Li-Ion Storage Application

Yunan Liu [1,2], Ting Sun [2], Duygu Ege [3] and Ali Reza Kamali [1,*]

[1] School of Metallurgy, Northeastern University, Shenyang 110819, China; 2310632@stu.neu.edu.cn
[2] College of Science, Northeastern University, Shenyang 110819, China; sunting@neu.edu.cn
[3] Institute of Biomedical Engineering, BoğaziçI University, 34684 Istanbul, Turkey; duygu.ege@boun.edu.tr
* Correspondence: ali@mail.neu.edu.cn or a.r.kamali@cantab.net

Abstract: Onion waste, particularly onion skin, is a widely generated waste material, and harnessing its potential for energy storage aligns with sustainable development goals. Despite the high specific surface area exhibited by biocarbon derived from onion skin, its Li-ion storage performance is not desirable. In this study, biocarbon derived from purple onion skin serves as the substrate for accommodating cobalt oxide (Co_3O_4) through a hydrothermal method, employing $Co(NO_3)_2{\cdot}6H_2O$ at various concentrations, and with and without prior activation using KOH treatment. The resulting samples undergo comprehensive analyses, including phase, morphological, surface, and electrochemical characterizations. The Co_3O_4 decoration on activated carbon derived from onion skin, synthesized using $Co(NO_3)_2{\cdot}6H_2O$ at a concentration of 1 M, reveals a porous structure with a surface area of 702 m^2/g, featuring predominant pore sizes of less than 5 nm. Significantly, the Li-ion storage performance of this sample surpasses that of alternative samples, demonstrating a remarkable reversible capacity of 451 mAh/g even after 500 cycles at an elevated current density of 2000 mAh/g. The charge transfer resistance of the sample (110.3 Ω) is found to be substantially lower than that of the sample prepared using carbonized onion skin biomass without activation. This research introduces an innovative approach leveraging onion skin waste as a template for Co_3O_4 decoration, thereby fabricating high-performance anodes for lithium-ion batteries.

Keywords: onion skin biomass; activation; Co_3O_4; lithium-ion battery; anode

Citation: Liu, Y.; Sun, T.; Ege, D.; Kamali, A.R. Cobalt Oxide-Decorated on Carbon Derived from Onion Skin Biomass for Li-Ion Storage Application. *Metals* **2024**, *14*, 191. https://doi.org/10.3390/met14020191

Academic Editor: Bernd Friedrich

Received: 28 December 2023
Revised: 22 January 2024
Accepted: 29 January 2024
Published: 2 February 2024

1. Introduction

Replacing fossil fuels with diverse clean and renewable energy sources is imperative to address the current energy crisis and environmental challenges [1]. In recent decades, lithium-ion electrochemical energy storage systems have experienced rapid advancements, achieving notable breakthroughs due to their compact size, extended life cycle, and lack of operational pollution [2,3]. Carbon materials play a prevalent role as the negative electrode in Li-ion batteries (LIBs) [4]. Nevertheless, their theoretical specific capacity is constrained to 372 mAh/g, limiting the overall performance [5]. Currently, developing electrode materials with both a highly specific capacity and robust cycle performance for LIBs remains a formidable task [6].

Biomass materials emerge as environmentally preferable alternatives to conventional electrode materials, owing to their low cost, widespread availability, and rapid regeneration. Various biomass materials derived from plants, animals, and microorganisms have been synthesized for diverse applications [7–11]. Notably, onions, the second most cultivated vegetable crop globally [12], contribute to this pool of biomass materials. Approximately 10% of onion products, mainly comprising onion skin, are discarded as waste directly into the environment [13]. This waste has found utility in the production of functional materials, such as bioactive agents [13], or as adsorbents for removing organic pollutants [14]. Furthermore, carbon derived from discarded onion skins exhibits a high specific surface

area and mesoporous structure, making it advantageous for applications such as supercapacitors [15,16]. Surprisingly, despite these attributes, the exploration of onion skin as a negative electrode for Li-ion batteries (LIBs) has been absent in the literature, and this research aims to fill that gap.

Transition metal oxides, including Sn [17,18], Mo [19–21], Cu [22,23], and Fe [24,25], have been investigated as anode materials for LIBs due to their high theoretical capacities and availability. Among these, Co_3O_4 stands out as a promising oxide with a theoretical capacity of 890 mAh/g [26,27]. However, the practical utilization of Co_3O_4 faces challenges related to significant volume changes during Li-ion insertion and extraction processes, as well as the poor electronic conductivity of this transitional metal oxide [28,29]. Various methods have been developed to address these issues, such as the fabrication of Co_3O_4 nanoparticles and nanowires [30–32], often combined with additional materials to facilitate the charge transfer. This configuration helps reduce the material volume variation and enhance electrochemical properties [33–35]. Incorporating carbon as an additional component in Co_3O_4-based anodes can lead to composite materials benefiting from the highly specific capacity of the transition metal oxide and the electrical conductivity of the carbon component [36,37]. For example, Li et al. [38] synthesized a Co_3O_4/C composite material using sodium alginate cobalt fibers, calcium chloride, and cobalt chloride as the raw materials employing an acid (HCl) treatment, followed by calcination at 800 °C. The material exhibited a Li-ion storage capacity of 782 mAh/g after cycles, at the current density of 89 mA/g.

However, these strategies often involve a complex synthesis or relatively high production costs, posing challenges to their practical applications [39]. For example, Chen et al. [40] wrapped zeolitic imidazolate frameworks containing tetrahedral Co cations in polyacrylonitrile by electrospinning, and calcined the compound at 700 °C for 2 h to prepare the Co/carbon nanofibers. Then, the sample was further calcined at 300 °C (6 h) to obtain Co_3O_4/carbon nanofibers, which experienced a vulcanization process at 450 °C to introduce sulfur to the system. The final product provided a capacity of 325 mAh/g at 10 A/g.

The exploration of a facile method for producing Co_3O_4/carbon composites using onion skin waste represents a compelling avenue in this research. In this investigation, onion skin waste serves as the carbon template, onto which Co_3O_4 is intricately deposited through a straightforward hydrothermal approach utilizing $Co(NO_3)_2 \cdot 6H_2O$. The resulting composite material is synthesized both without the activation of the carbonized onion skin (COS) and, alternatively, after the activation of the carbon material (A-COS). This leads to the preparation of two distinct materials, namely Co-COS and Co-A-COS. Subsequently, these materials are subjected to comprehensive characterization through various techniques. In particular, this study introduces a novel strategy for the utilization of onion skin waste in the fabrication of Co_3O_4 composites tailored for efficient Li-ion storage. By delving into the unexplored territory of utilizing onion skin waste, this research not only addresses environmental concerns related to waste biomass disposal but also offers a sustainable and cost-effective solution for the production of advanced materials for energy storage applications. The characterization of Co-COS and Co-A-COS materials aims to elucidate their structural, morphological, and electrochemical properties, contributing insights to the development of onion skin waste-derived materials for energy storage applications. Through these efforts, this research contributes to the ongoing exploration of green and sustainable approaches in material synthesis and energy storage technologies [41].

The novelty of the current work lies in the innovative approach of utilizing onion skin waste as a template for the decoration of cobalt oxide (Co_3O_4) crystals. This process involves a hydrothermal method, utilizing $Co(NO_3)_2 \cdot 6H_2O$ at various concentrations, with and without prior activation using the KOH treatment. The resulting composite material, synthesized from the activated carbon derived from onion skin, demonstrates enhanced Li-ion storage electrochemical performances. The sample synthesized with $Co(NO_3)_2 \cdot 6H_2O$ at a concentration of 1 M shows a superior Li-ion storage performance with a remarkable reversible capacity of 451 mAh/g, even after 500 cycles at an elevated current density of 2000 mAh/g.

2. Experimental Section

2.1. Material Synthesis

The purple onion skin biomass was washed by deionized water and dried in an oven at 60° for 24 h. The dried onion skins were then carbonized by heating in a tube furnace under a nitrogen protective gas at the heating rate of 5 °C/min to 700 °C with a dwell time at a maximum temperature of 2 h. Then, the carbonized onion skin (COS) and KOH were mixed by mass ratio of 1:4, and the mixture was dried for 24 h at 60°, before being thermally treated under nitrogen at 800 °C for 1 h at a heating rate of 5 °C/min. The solid material obtained (1 g) was added into 100 mL hydrochloric acid (1 M), and the suspension was stirred for 24 h. Subsequently, the suspension was filtered, and the filtrate was washed with deionized water to fully remove the acid, in order to prepare the activated carbonized onion skin (A-COS). Then, the A-COS was loaded with cobalt oxide. For this, COS and A-COS were separately added into a solution of $Co(NO_3)_2{\cdot}6H_2O$ with varying concentrations of 0.5, 1, and 1.5 M. Then, the suspensions were heated in an autoclave at 180 °C for 20 h to prepare the final samples, namely Co-A-COS (0.5 M), Co-A-COS (1.0 M) and Co-A-COS (1.5 M). Figure 1 exhibits the method employed to fabricate various samples. Additionally, the COS sample was used without activation to interact with $Co(NO_3)_2{\cdot}6H_2O$ (1 M) in the autoclave. This sample is called Co-COS (1 M).

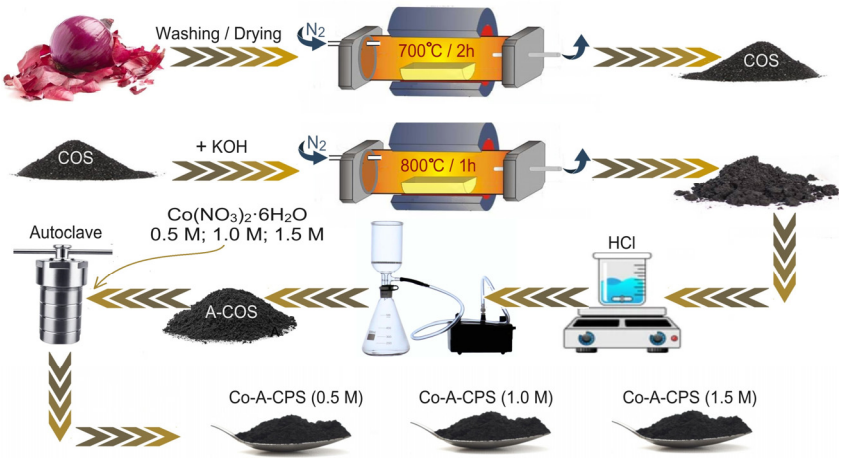

Figure 1. Schematic representation of the process employed to prepare samples.

2.2. Material Characterization

The phase characterization was conducted using an X-ray powder diffraction employing Cu-K_α radiation with a step size of 0.03 using an X'Pert Pro diffractometer (Panaco, The Netherlands). Thermogravimetric analysis (TGA) was conducted under nitrogen atmosphere at a heating rate of 5 °C/min using a thermal analyzer (Mettler Toledo, UK). A field emission scanning electron microscope (SSX-550, Shimadzu, Japan) was used for morphological characterization. A Micromeritics ASAP 2020 HD88 instrument (Germany) was used for surface characterizations.

2.3. Cell Assembling and Electrochemical Characterization

Li-ion half-cells were assembled using biocarbon-derived materials. For this, N-methylpyrrolidone (NMP) was used as solvent, using which a slurry was made employing the active material (80%), acetylene black (10%), and polyvinylidene fluoride (PVDF) binder (10%). To this end, PVDF was mixed with NPM in a mass ratio of 1:9, and the mixture was stirred vigorously until it became transparent. Then, the acetylene black and the active material were added; the suspension obtained was subjected to grinding using a mortar and pestle to make the slurry, which was subsequently coated on copper foil. For coating, a piece of copper foil was fixed onto a cleaned glass, and then, the slurry was evenly spread onto the copper foil using the doctor blade method. The coated foil was then dried in a vacuum oven at 120 °C for more than 8 h. The electrodes were assembled into 2032 coin cells using 1 M

$LiPF_6$ in EC:DMC (1:1 vol) as the electrolyte, as well as the polypropylene (PP) Celgard 2400 membrane as the separator, in an argon-filled glove box. The active material mass loading was measured to be 0.9 mg/cm^2–1.3 mg/cm^2. A CT2001A (LAND Electronic, Wuhan Jinnuo Electronics) was used for galvanostatic discharge-charge measurements within the range of 0.01–3 V. The cyclic voltammetry (CV) curves were measured using an electrochemical workstation (CHI760E) at the rate of 0.1 mv/S.

3. Results and Discussion

3.1. Structural, Morphological, Thermal, and Surface Characterization

Figure 2a represents the X-ray diffraction patterns of Co-COS (1 M) and Co-A-COS (1 M), prepared based on the method exhibited in Figure 1. The XRD pattern on Co-A-COS (1 M), shown in Figure 2a, confirms the presence of Co_3O_4 as the major phase. In particular, the diffraction peaks located at the two-theta values of 31.68°, 36.7°, 44.6°, 59°, and 65° could be assigned to the (202), (311), (500), (811), and (904) crystalline planes of the spinel-structured cubic Co_3O_4. Similarly, the XRD pattern of the Co-COS (1 M), shown in Figure 2a, demonstrates the presence of Co_3O_4. As can be observed, the diffraction peaks of Co_3O_4 in Co-A-COS (1 M) are sharper and narrower than those of Co-COS (1 M), indicating that the Co_3O_4 phase decorated on the activated carbonized onion skin (A-COS) has a greater crystallinity than the one fabricated using a non-activated material sample (COS).

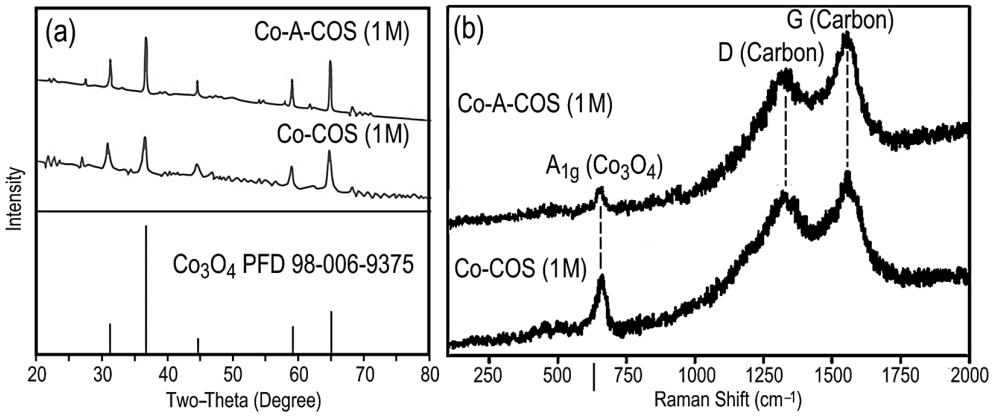

Figure 2. (**a**) XRD patterns and (**b**) Raman spectra of Co-A-COS (1 M) and Co-COS (1 M).

The Raman spectra of both Co-COS (1 M) and Co-A-COS (1 M) are illustrated in Figure 2b. Notably, the initial prominent Raman peak detected at approximately 670 cm^{-1} in both samples can be attributed to the A_{1g} phonon mode in Co_3O_4 [42,43]. Additionally, the Raman bands observed at approximately 1337 and 1559 cm^{-1} correspond to the D and G bands often observed in defective graphitic structures [44,45], indicative of the A_{1g} and E_{2g} vibrational modes of the biomass-derived carbon, respectively, within the Co_3O_4/C nanocomposites. The D band signifies the presence of sp^3-hybridized, disordered carbon [46], along with other structural defects, while the G band represents the sp^2 -hybridized carbon in an ordered graphite structure [47].

The ratio of the intensities of the D and G bands (I_D/I_G) serves as a metric for the degree of graphitization in carbon materials [48]. The I_D/I_G ratio for the Co-A-COS (1 M) and Co-COS (1 M) composite materials is recorded at 0.75 and 0.83, respectively, confirming the defective graphitic structure of the biocarbon in these materials. This carbon structure provides a conductive platform for the integration of Co_3O_4 nanoparticles, thereby enhancing the Li-ion storage performance of the composite material.

The scanning electron microscopy (SEM) micrographs of the samples depicted in Figure 2 are presented in Figure 3. As illustrated in Figure 3a,b, the carbonized onion skin (COS) exhibits a flaky structure, while the activated carbonized onion skin (A-COS) displays significantly greater porosity, resulting in a larger specific surface area (Figure 3b,c).

These findings suggest that the activation process enhances the porosity and surface area of the resulting carbon material. This is in agreement with other studies confirming the formation of a highly carbon porous structure through a KOH activation step involving the melting and penetration of KOH into the carbon structure [49].

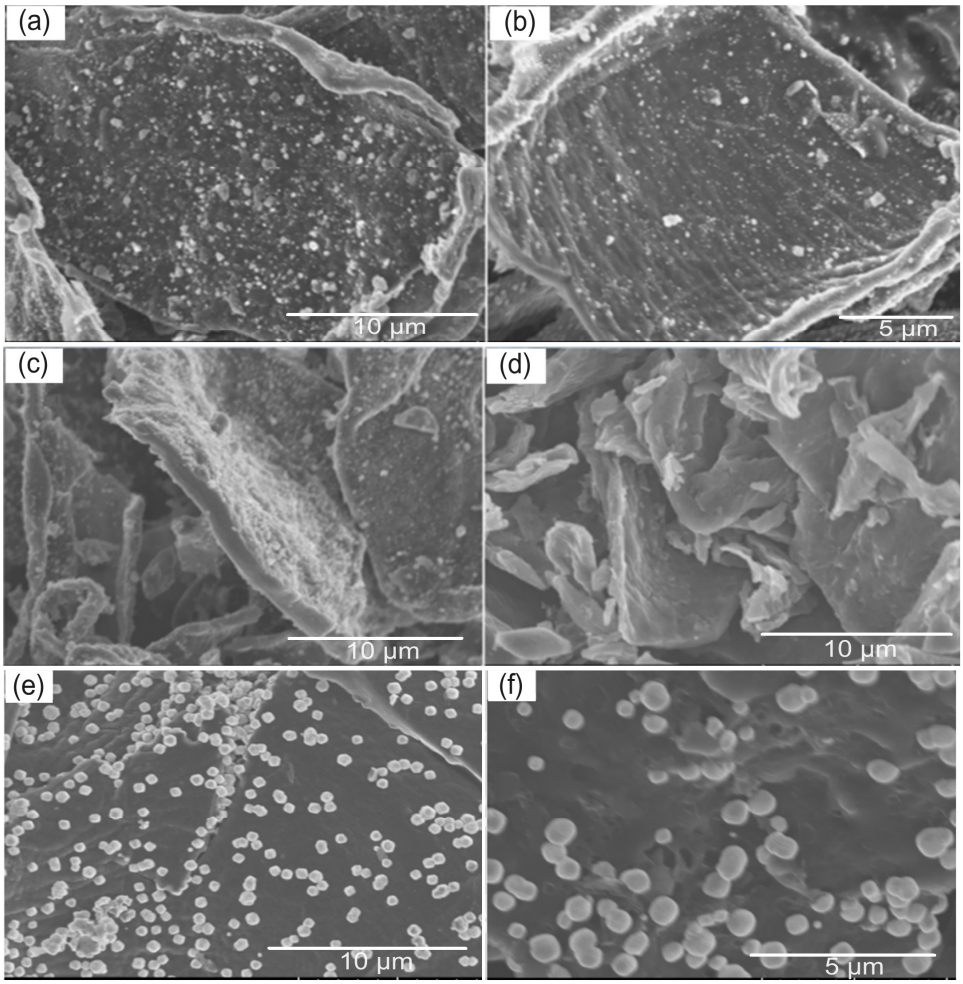

Figure 3. SEM micrographs of the (**a**,**c**) COS, (**b**,**d**) A-COS, (**e**) Co-COS (1 M), and (**f**) Co-A-COS (1 M).

Figure 3e illustrates the SEM morphology of Co-COS (1 M), revealing the presence of Co_3O_4 crystals deposited in the carbon substrate. A similar morphology is observed for Co-A-COS (1 M), with the distinction that the carbon substrate in the latter is rougher than that in the former.

The improved porous structure in A-COS inevitably facilitates the ion and electron transfer across the electrode, thereby enhancing the Li-ion storage capacity of the material, as elaborated in the article. Such structures also offer the increased access to transition metal oxide nanoparticles, thereby improving the electrochemical properties of the hybrid structure. In other words, both the carbonized onion skin (COS) and the activated COS can serve as templates for the deposition of Co_3O_4 while maintaining their structural integrity. The enhanced porous structure increases accessibility to the structure for the electrolyte, specifically lithium cations, when utilized as the anode in Li-ion batteries.

Energy-dispersive X-ray spectroscopy (EDS) was utilized to examine the distribution of various elements in the materials, and the corresponding results are depicted in Figure 4. These findings validate the existence of cobalt oxide nanoparticles on the carbon phase, corroborating the XRD patterns presented in Figure 2. The micrographs further reveal the uniform distribution of these nanoparticles.

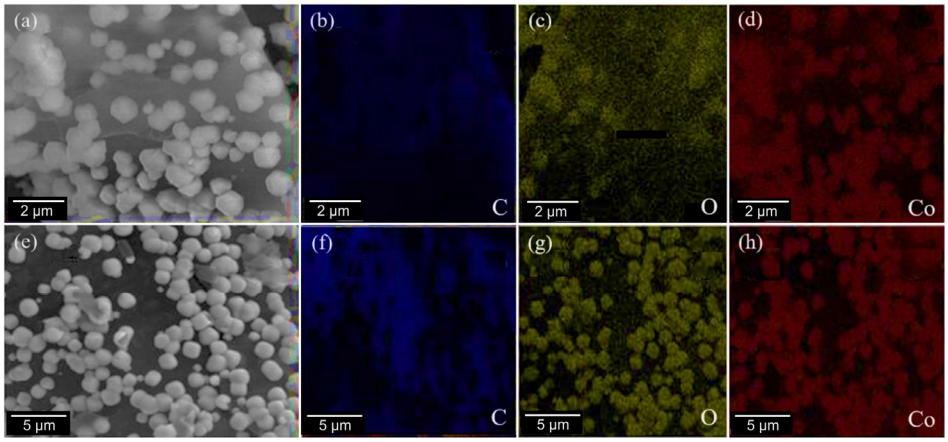

Figure 4. (**a**) SEM and EDS mapping analysis of (**a**–**d**) Co-COS (1 M) and (**e**–**h**) Co-A-COS (1 M).

The surface characteristics of Co-COS (1 M) and Co-A-COS (1 M) are illustrated in Figure 5. Figure 5a displays the N_2 adsorption-desorption isotherm hysteresis of Co-A-COS, revealing Type II isotherms with an H4 loop, according to the IUPAC classification [50]. Such isotherms are typically associated with physisorption on porous structures, indicating micro-mesoporous materials. The specific surface area of Co-A-COS (1 M) was determined to be 702 m^2/g. Figure 6b indicates that the predominant pore sizes fall within the range of less than 5 nm. The N_2 adsorption-desorption isotherms of Co-COS are presented in Figure 5c, displaying type III isotherms with H3-type hysteresis, indicating the presence of a porous structure. The majority of pore volume is attributed to pores with diameters in the range of 10–25 nm (Figure 5d). The specific surface area of Co-COS was found to be significantly smaller than that of Co-A-COS at 100 m^2/g. These findings underscore the greater porosity of Co-A-COS, which is consistent with the microscopy observations. The substantial porosity of the sample, coupled with the presence of Co_3O_4 nanoparticles, can enhance the kinetics of the Li-ion insertion and extraction into/out of the material, as discussed in the following section.

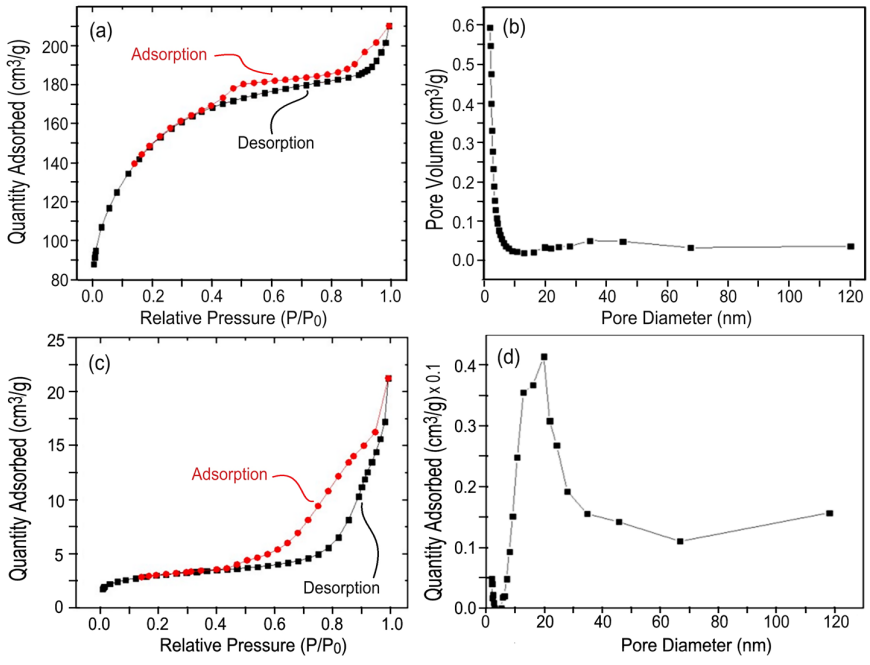

Figure 5. Nitrogen adsorption–desorption isotherm curves of (**a**) Co-A-COS and (**c**) Co-COS. Barret–Joyner–Halenda (BJH) pore size distribution curves of (**b**) Co-A-COS and (**d**) Co-COS.

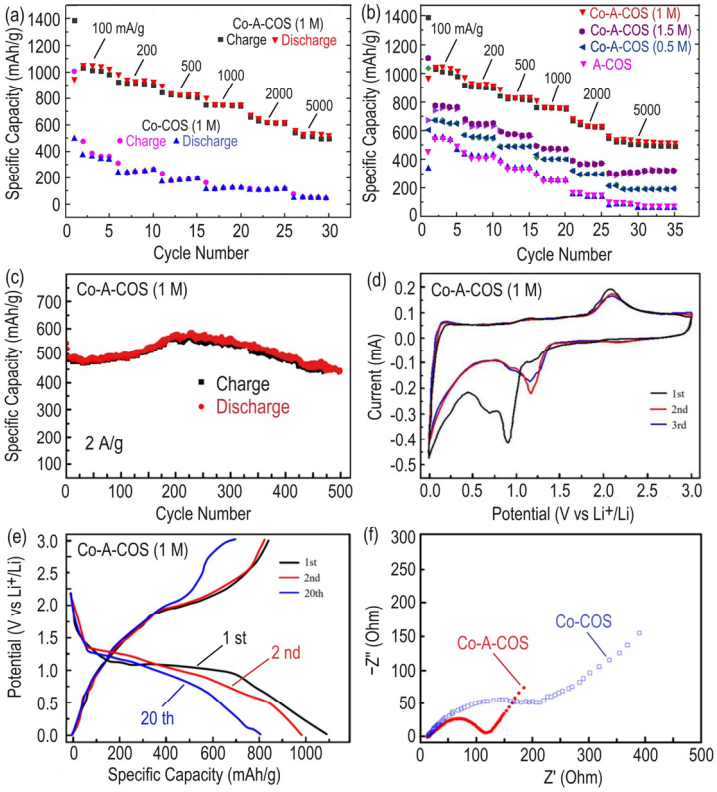

Figure 6. (**a**,**b**) Rate performances of various samples. (**c**) Cycling performance at 2000 mA/g, (**d**) CV, and (**e**) GCD curves of Co-A-COS (1 M). (**f**) EIS curves of Co-A-COS (1 M) and Co-COS (1 M).

3.2. Electrochemical Characterizations

The electrochemical performances of onion skin carbons decorated with Co_3O_4 as the anode in Li-ion batteries were assessed. Shown in Figure 6a, the Li-ion storage performances of Co-COS (1 M) and Co-A-COS (1 M) are compared at various current densities (100, 200, 500, 1000, 2000, and 5000 mA/g). Co-A-COS (1 M) demonstrates a discharge capacity of 1050 mAh/g at a current density of 100 mA/g after 5 cycles, surpassing the 502 mAh/g recorded for Co-COS (1 M) under the same conditions. Notably, the specific capacities of Co-A-COS (1 M) consistently outperform those of Co-COS (1 M) at higher current densities, reaching around 505 mAh/g after 30 cycles at 5000 mA/g, while that of Co-COS (1 M) is limited to approximately 90 mAh/g under this high current density.

Co-A-COS samples were synthesized through the hydrothermal treatment of A-COS and $Co(NO_3)_2{\cdot}6H_2O$ with varying concentrations of 0.5, 1, and 1.5 M. The impact of these concentrations on the Li-ion storage performance of the resulting hybrid nanostructures is explored in Figure 6b. At the current density of 100 mA/g, the capacities after 5 cycles for A-COS, Co-A-COS (0.5 M), Co-A-COS (1 M), and Co-A-COS (1.5 M) were recorded as 491, 623, 1050, and 780 mAh/g, respectively. This trend persists at higher current densities, providing evidence for the superior performance of Co-A-COS (1 M) compared to other samples.

To further evaluate the electrochemical performance of Co-A-COS (1 M), the prolonged Li-ion storage cycling performance of the material was examined at the current density of 2000 mA/g (Figure 6c). As shown, the capacity of the sample experienced an initial decline which is due to the decomposition of the electrolyte onto the electrode, leading to the formation of the solid electrolyte interphase (SEI) [51]. Then, the capacity of the sample gradually increases to record a value of around 550 mAh/g after 220 cycles, after which the capacity gradually decreases to exhibit a value of 451 mAh/g after 500 cycles. Figure 7 shows the Coulombic efficiency (CE) of the Co-A-CoS (1M) electrode at the current density of 2 A/g. As can be observed, the CE at the first cycle is around 76.5%, which increases to around 90 and 95% at the second and third cycle cycles, respectively, and eventually to

more than 98% after 20 Li-ion insertion/extraction cycles. This value is recorded to be 99.3% after 500 cycles. The lower CE at initial cycles can mainly be related to the formation of SEI layers. However, the initial Coulombic efficiency (76.5%) is still relatively high, indicating an appropriate degree of electrochemical stability right from the first cycle, which is an important parameter in practical applications [52].

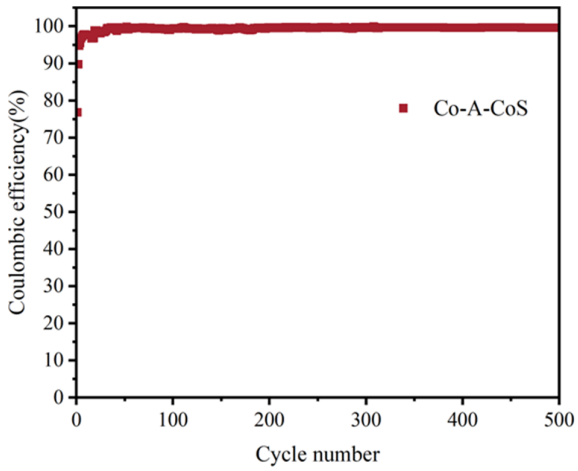

Figure 7. Coulombic efficiency of Co-A-CoS (1M) at the current density of 2 A/g.

As observed in Figure 6c, after around 20 cycles, the capacity of the electrode experiences a rising trend until the 220th cycle. This phenomenon can be attributed to the activation of electrode materials during the charge-discharge processes. This behavior has also been reported for the case of other oxide electrodes, where the detailed mechanism involved is still unclear [53]. However, the origin of this cycling-induced capacity-increase after a certain number of cycles [54] can be related to a combination of reasons, including the gradual amorphization of the electrode after cycling, and the formation of metallic components due to the partially irreversible conversion mechanism, lowering the activation overpotential involved in Li-ion insertion and extraction [54].

Moreover, the decrease in the capacity observed after 220 cycles (Figure 6c) can be related to various issues, including the large volume changes involved in Li-ion insertion/extraction into/out of the electrode [55].

To shed light on the Li-ion storage mechanism of Co-A-COS (1 M), cyclic voltameter measurements were performed at 0.01–3.00 V (Figure 6d).

During the first cathodic scan, three cathodic peaks can be observed at around 0.9, 0.4 V, and less than 0.1 V. The reduction peaks at 0.9 and 0.4 V are related to the combination of forming SEI and the reduction of Co_3O_4 to form Co [56]:

$$Co_3O_4 + 8Li^+ + 8e^- \rightarrow 3Co + 4Li_2O \quad (1)$$

Accordingly, the anodic peak observed at around 2.2 V is related to the oxidation of Co to CoO:

$$Co + Li_2O \rightarrow CoO + 2Li^+ + 2e^- \quad (2)$$

The cathodic peak observed in the first cycle below 0.1 V is accompanied by an anodic peak. This event can be related to the insertion and extraction of Li^+ into/out of the activated carbon obtained by the carbonization of the biomass. The cathodic peak at 0.9 V moves to a greater potential of 1.2 V in the second cycle, corresponding to the reduction of CoO:

$$CoO + 2Li^+ + 2e^- \rightarrow Co + Li_2O \quad (3)$$

However, the corresponding anodic peak does not move in comparison to that of the first cycle, confirming the occurrence of the oxidation reaction based on the reversible reac-

tion (2). The curves of the second and third cycles correlate well, indicating the reversibility of the electrochemical reactions. This mechanism can be confirmed by considering the galvanostatic charge-discharge curves recorded at 100 mA/g (Figure 6e).

As can be observed, the specific capacities of the material at the first discharge and after 20 cycles could reach around 1100 and 800 mAh/g, respectively. In the first cycle, the specific capacities of the material under the charge and discharge were 960 and 1200 mAh/g, respectively, with the coulombic efficiency of around 80%. At the 20th cycle, the specific capacities of the charge and discharge processes were 760 and 800 mAh/g, respectively, with the coulombic efficiency of greater than 95%.

As shown in Figure 6, the enhanced performance of Co-A-COS (1 M) in comparison with that of Co-COS (1 M) is evident, and this enhancement was related to the greater porous structure of the earlier, brought about by the activation process. The greater prosity of Co-A-COS (1 M) could facilitate the ion transportation of the electrode/electrolyte interface, leading to a reduced charge transfer resistance, as demonstrated by the EIS curves shown in Figure 6f. The EIS curves show one high frequency semi-circle and a low frequency line corresponding to the charge-transfer process and the semi-infinite linear mass-transport of the ions, respectively [57]. The diameter of the semi-circle and slope of the line represent the charge transfer resistance and the diffusion resistance, respectively. It can be clearly observed from Figure 6f that the charge resistance of Co-A-COS (110.3 Ω) is significantly lower than that of Co-COS (245.1 Ω).

In this research, onion skin as a widely available biomass was used to extract carbon materials (COS) which were subsequently decorated with Co_3O_4 nanocrystals, using $Co(NO_3)_2{\cdot}6H_2O$ of various concentrations, with and without being activated beforehand. The sample obtained using the activated carbon with a $Co(NO_3)_2{\cdot}6H_2O$ concentration of 1 M (Co-A-COS (1M)) demonstrated an enhanced Li-ion storage performance, as illustrated by a capacity of 451 mAh/g even after 500 cycles at the enhanced current density of 2000 mA/g. This performance can be compared with the literature including the work of Huang et al. [56], who fabricated mesoporous Co_3O_4 nano-cubes. This sample could exhibit a capacity of 400 mAh/g at 2000 mAh/g after 60 cycles where the cycling was terminated. The electrochemical performance of Co-A-CoS (1 M), in contrast with alternative materials from the literature, is summarized in Table 1, highlighting the superior Li-ion storage performance of the CoA-CoS (1 M) composite material. As shown, at a high current density of 2000 mA/g and after 200 cycles, the electrode exhibits a capacity of 571 mAh/g, which is the highest value among the materials presented in the table tested at lower current densities in the range from 20 to 1000 mA/g. After 500 cycles, the CoA-CoS (1 M) electrode retains a high capacity of 450 mAh/g, which is indicative of its resilience and consistent energy delivery; this is critical for practical applications. From Table 1, at the current density of 100 mA/g, the capacity of pure Co_3O_4 decreases from an initial value of 1387 mA h g^{-1} to a limited capacity of 115 mAh/g after 100 cycles [58], providing evidence for the efficiency of carbon components in maintaining the capacity at prolonged cycles [59–61].

Table 1. Electrochemical performance of samples prepared in the current study in contrast with alternative materials extracted from the literature.

Active Material	Current Density (mA/g)	Capacity (mAh/g)	Cycle	Reference
Co_3O_4	100	115	100	[58]
CNT/Co_3O_4	200	498	100	[59]
C/Co_3O_4-nanowires	20	534	100	[60]
Graphene/Co_3O_4	1000	550	100	[61]
Co-A-CoS (1 M)	2000	578	200	This work
Co-A-CoS (1 M)	2000	451	500	This work

In the current work, CO_3O_4 crystals decorated on carbon were fabricated using onion skin waste, and the material obtained was employed to fabricate anode materials for Li-ion

storage with a high capacity and stability over cycling. This strategy not only facilitates the preparation of high-performance energy materials but also actively contributes to ongoing research focused on the sustainable utilization of waste [62,63]. Along with the green utilization of natural resources [64,65], the successful implementation of waste-to-energy solutions [66,67] represents a crucial stride toward achieving the sustainable development goals, advocating for the efficient recycling and valorization of waste. Additional research can be directed to investigate the impact of carbon derived from onion skin on enhancing the electrochemical performance of hybrid nanostructures. Furthermore, exploring various applications of this biomass-derived carbon, such as water treatment [68,69], biomedical applications [70,71], modern metallurgical processes [72,73], and catalysis [74], merits attention in forthcoming research endeavors.

It should be noted that cobalt is recognized as a crucial element for various applications, including serving as the cathode in Li-ion batteries, as well as being utilized in electronics, superalloys, and hard metals. Consequently, effective cobalt recycling [75] can be considered a viable source for secondary applications, such as in the anode of Li-ion batteries, as discussed in this article. The Li-ion performance of Co-A-CoS (1 M) may be influenced by other parameters, such as the electrolyte components. Additionally, the presence of impurities in biomass and their variability depending on the environment warrants further investigation in future studies. Novel technologies, such as reserve lithium-ion batteries [76], and strategies developed to mitigate voltage hysteresis in reversed conversion reactions of transitional metal oxide anodes [77], could be utilized to enhance the performance of Co-A-CoS electrodes in future studies. Another application of the C-A-COS electrodes is their use as a lithiophilic magnetic host matrix, aiming to simultaneously mitigate uncontrolled dendritic lithium growth and substantial lithium volume expansion, which are common challenges in typical lithium-metal anodes used in LIBs [78].

4. Conclusions

In this investigation, carbon derived from onion skin biomass (COS) served as the template for adorning Co_3O_4, with and without the prior activation of the biocarbon. The resulting samples underwent comprehensive analyses, encompassing phase, morphological, surface, and electrochemical characterizations. The Co_3O_4 decoration on activated carbon derived from onion skin, synthesized using $Co(NO_3)_2 \cdot 6H_2O$ with a concentration of 1 M, led to the production of a porous structure with the surface area of 702 m^2/g with predominant pore sizes of less than 5 nm. Notably, the Li-ion storage performance of this sample outperformed alternative samples, exhibiting a remarkable reversible capacity of 451 mAh/g even after 500 cycles at an elevated current density of 2000 mAh/g. The charge transfer resistance of the sample (110.3 Ω) was found to be significantly lower than that of the sample prepared using carbonized onion skin biomass without activation. This research introduces an innovative approach utilizing onion skin waste as a template for Co_3O_4 crystal decoration, thereby fabricating high-performance anodes for lithium-ion batteries.

Author Contributions: Conceptualization, Y.L. and T.S.; methodology, Y.L. and T.S.; validation, Y.L., T.S. and A.R.K.; formal analysis, Y.L., T.S. and A.R.K.; investigation, Y.L., T.S. and A.R.K.; resources, Y.L., T.S., D.E. and A.R.K.; data curation, Y.L., T.S. and A.R.K.; writing—original draft preparation, Y.L. and A.R.K.; writing—review and editing, A.R.K.; visualization, Y.L. and A.R.K.; supervision, T.S. and A.R.K.; project administration, Y.L., T.S., D.E. and A.R.K.; funding acquisition, T.S. and A.R.K. All authors have read and agreed to the published version of the manuscript.

Funding: Financial support by National Natural Science Foundation of China (52250610222) is acknowledged.

Data Availability Statement: The raw data supporting the conclusions of this article will be made available by the authors on request.

Conflicts of Interest: The authors declare no conflicts of interest.

References

1. Zhao, X.; Gao, P.; Shen, B.; Wang, X.; Yue, T.; Han, Z. Recent advances in lignin-derived mesoporous carbon based-on template methods. *Renew. Sustain. Energy Rev.* **2023**, *188*, 113808. [CrossRef]
2. Poorshakoor, E.; Darab, M. Advancements in the development of nanomaterials for lithium-ion batteries: A scientometric review. *J. Energy Storage* **2024**, *75*, 109638. [CrossRef]
3. Liu, F.; Yu, D.; Shao, C.; Liu, X.; Su, W. A review of multi-state joint estimation for lithium-ion battery: Research status and suggestions. *J. Energy Storage* **2023**, *73*, 109071. [CrossRef]
4. Shabir, A.; Hashmi, S.A.; Hor, A.A.; Julien, C.M.; Islam, S.S. Long-term prospects of nano-carbon and its derivatives as anode materials for lithium-ion batteries—A review. *J. Energy Storage* **2023**, *72*, 108178. [CrossRef]
5. Zhong, C.; Weng, S.; Wang, Z.; Zhan, C.; Wang, X. Kinetic limits and enhancement of graphite anode for fast-charging lithium-ion batteries. *Nano Energy* **2023**, *117*, 108894. [CrossRef]
6. Muchuweni, E.; Mombeshora, E.T.; Muiva, C.M.; Sathiaraj, T.S. Lithium-ion batteries: Recent progress in improving the cycling and rate performances of transition metal oxide anodes by incorporating graphene-based materials. *J. Energy Storage* **2023**, *73*, 109013. [CrossRef]
7. Grira, S.; Alkhedher, M.; Abu Khalifeh, H.; Ramadan, M.; Ghazal, M. Using algae in Li-ion batteries: A sustainable pathway toward greener energy storage. *Bioresour. Technol.* **2024**, *394*, 130225. [CrossRef]
8. Li, R.; Kamali, A.R. Molten salt assisted conversion of corn lignocellulosic waste into carbon nanostructures with enhanced Li-ion storage performance. *Chem. Eng. Sci.* **2023**, *265*, 118222. [CrossRef]
9. Santos, B.L.P.; Vieira, I.M.M.; Ruzene, D.S.; Silva, D.P. Unlocking the potential of biosurfactants: Production, applications, market challenges, and opportunities for agro-industrial waste valorization. *Environ. Res.* **2024**, *244*, 117879. [CrossRef]
10. Mannaa, M.; Mansour, A.; Park, I.; Lee, D.W.; Seo, Y.S. Insect-based agri-food waste valorization: Agricultural applications and roles of insect gut microbiota. *Environ. Sci. Ecotechnol.* **2024**, *17*, 100287. [CrossRef]
11. Sennu, P.; Aravindan, V.; Lee, Y.S. High energy asymmetric supercapacitor with 1D@2D structured $NiCo_2O_4$@Co_3O_4 and jackfruit derived high surface area porous carbon. *J. Power Sources* **2016**, *306*, 248–257. [CrossRef]
12. Han, L.J.; Zhang, P.; Li, L.; Lu, S.Q.; Su, B.T.; An, X.C.; Lei, Z.Q. Nitrogen-containing carbon nano-onions-like and graphene-like materials derived from biomass and the adsorption and visible photocatalytic performance. *Appl. Surf. Sci.* **2021**, *543*, 148752. [CrossRef]
13. Cruz, E.P.; Jansen, E.T.; Costa, L.V.; Souza, E.J.D.; Fonseca, L.M.; Gandra, E.A.; Zavareze, E.R.; Dias, A.R.G. Use of red onion skin (*Allium cepa* L.) in the production of bioactive extract and application in water-absorbing cryogels based on corn starch. *Food Hydrocoll.* **2023**, *145*, 109133. [CrossRef]
14. Adeola, A.O.; Oyedotun, K.O.; Waleng, N.J.; Mamba, B.B.; Nomngongo, P.N. Onion skin–derived sorbent for the sequestration of methylparaben in contaminated aqueous medium. *Biomass Convers. Biorefin.* **2023**. [CrossRef]
15. Zhu, H.L.; Jia, Z.; Chen, Y.C.; Weadock, N.; Wan, J.Y.; Vaaland, O.; Han, X.G.; Li, T.; Hu, L.B. Tin anode for sodium-ion batteries using natural wood fiber as a mechanical buffer and electrolyte reservoir. *Nano Lett.* **2013**, *13*, 3093–3100. [CrossRef] [PubMed]
16. Wang, D.W.; Liu, S.J.; Fang, G.L.; Geng, G.H.; Ma, J.F. From trash to treasure: Direct transformation of onion husks into three-dimensional interconnected porous carbon frameworks for high performance supercapacitors in organic electrolyte. *Electrochim. Acta* **2016**, *216*, 405–411. [CrossRef]
17. Yu, J.; Gao, L.Z.; Li, X.L.; Wu, C.; Gao, L.L.; Li, C.M. Porous carbons produced by the pyrolysis of green onion leaves and their capacitive behavior. *New Carbon Mater.* **2016**, *31*, 475–484. [CrossRef]
18. Li, S.; Kamali, A.R. Molten salt-assisted valorization of waste PET plastics into nanostructured SnO_2@terephthalic acid with excellent Li-ion storage performance. *Appl. Energy* **2023**, *334*, 120692.
19. Zhu, W.H.; Kamali, A.R. Molten Salt-Assisted Catalytic Preparation of MoS_2/α-MoO_3/Graphene as High-Performance Anode of Li-Ion Battery. *Catalysts* **2023**, *13*, 499. [CrossRef]
20. Zhu, W.H.; Kamali, A.R. Thermal oxidation of MoS_2 into defective crystalline MoO_3 with enhanced Li-ion storage kinetics. *J. Alloys Compd.* **2023**, *968*, 171823. [CrossRef]
21. Zhu, W.H.; Kamali, A.R. Green preparation of nanostructured β-MoO_3/hexagonal-shaped MoS_2/graphene with enhanced lithium-ion storage performance. *J. Alloys Compd.* **2023**, *932*, 167724. [CrossRef]
22. Park, J.C.; Kim, J.; Kwon, H.; Song, H. Gram-scale synthesis of Cu_2O nanocubes and subsequent oxidation to CuO hollow nanostructures for lithium-ion battery anode materials. *Adv. Mater.* **2009**, *21*, 803–807. [CrossRef]
23. Li, Z.F.; Xie, G.M.; Wang, C.X.; Liu, Z.J.; Chen, J.; Zhong, S.W. Binder free Cu_2O/CuO/Cu/Carbon-polymer composite fibers derived from metal/organic hybrid materials through electrodeposition method as high performance anode materials for lithium-ion batteries. *J. Alloys Compd.* **2021**, *864*, 158585. [CrossRef]
24. Chen, Y.; Xia, H.; Lu, L.; Xue, J.M. Synthesis of porous hollow Fe_3O_4 beads and their applications in lithium ion batteries. *J. Mater. Chem.* **2012**, *22*, 5006–5012. [CrossRef]
25. Li, L.; Wang, H.L.; Xie, Z.J.; An, C.H.; Jiang, G.X.; Wang, Y.J. 3D graphene-encapsulated nearly monodisperse Fe_3O_4 nanoparticles as high-performance lithium-ion battery anodes. *J. Alloys Compd.* **2020**, *815*, 152337. [CrossRef]
26. Liu, J.; Xia, H.; Lu, L.; Xue, D.F. Anisotropic Co_3O_4 porous nanocapsules toward high-capacity Li-ion batteries. *J. Mater. Chem.* **2010**, *20*, 1506–1510. [CrossRef]

27. Zhao, Y.C.; Liu, C.G.; Yi, R.W.; Li, Z.Q.; Chen, Y.B.; Li, Y.Q.; Mitrovic, I.; Taylor, S.; Chalker, P.; Yang, L. Facile preparation of Co_3O_4 nanoparticles incorporating with highly conductive MXene nanosheets as high-performance anodes for lithium-ion batteries. *Electrochim. Acta* **2020**, *345*, 136203. [CrossRef]
28. Lou, Y.B.; He, D.; Wang, Z.F.; Hu, Y.H.; Shen, Y.; Ming, J.; Chen, J.X. Nanocomposite of ultrasmall Co_3O_4 nanoparticles deposited on ultrathin MoS_2 surfaces for excellent performance anode materials in lithium ion batteries. *Chem. Eng. J.* **2017**, *313*, 1269–1277. [CrossRef]
29. Ji, L.W.; Lin, Z.; Alcoutlabi, M.; Zhang, X.W. Recent developments in nanostructured anode materials for rechargeable lithium-ion batteries. *Energy Environ. Sci.* **2011**, *4*, 2682–2699. [CrossRef]
30. Xia, X.H.; Tu, J.P.; Mai, Y.J.; Wang, X.L.; Gu, C.D.; Zhao, X.B. Self-supported hydrothermal synthesized hollow Co_3O_4 nanowire arrays with high supercapacitor capacitance. *J. Mater. Chem.* **2011**, *21*, 9319–9325. [CrossRef]
31. Chen, H.H.; He, J.; Li, Y.L.; Luo, S.; Sun, L.N.; Ren, X.Z.; Deng, L.B.; Zhang, P.X. Hierarchical CuO_x-Co_3O_4 heterostructure nanowires decorated on 3D porous nitrogen-doped carbon nanofibers as flexible and free-standing anodes for high-performance lithium-ion batteries. *J. Mater. Chem.* **2019**, *A7*, 7691–7700. [CrossRef]
32. Huang, H.; Zhu, W.J.; Tao, X.Y.; Xia, Y.; Yu, Z.Y.; Fang, J.W.; Gan, Y.P.; Zhang, W.K. Nanocrystal-constructed mesoporous single-crystalline Co_3O_4 nanobelts with superior rate capability for advanced lithium-ion batteries. *ACS Appl. Mater. Interfaces* **2012**, *4*, 5974–5980. [CrossRef] [PubMed]
33. Bruce, P.G.; Scrosati, B.; Tarascon, J.M. Nanomaterials for rechargeable lithium batteries. *Angew. Chem. Int. Ed.* **2008**, *47*, 2930–2946. [CrossRef] [PubMed]
34. Guo, Y.G.; Hu, J.S.; Wan, L.J. Nanostructured materials for electrochemical energy conversion and storage devices. *Adv. Mater.* **2008**, *20*, 2878–2887. [CrossRef]
35. Kim, M.G.; Cho, J. Reversible and high-capacity nanostructured electrode materials for Li-ion batteries. *Adv. Funct. Mater.* **2009**, *19*, 1497–1514. [CrossRef]
36. Liu, M.; Li, H.; Yu, J.; Zhang, S.; Chen, Q.; Lu, W.; Yuan, A.; Zhong, L.; Sun, L. Hierarchical structure promoted lithiation/delithiation behavior of a double-carbon microsphere supported nano-Co_3O_4 anode. *Nanoscale* **2024**. [CrossRef] [PubMed]
37. Choi, B.G.; Chang, S.J.; Lee, Y.B.; Bae, J.S.; Kim, H.J.; Huh, Y.S. 3D heterostructured architectures of Co_3O_4 nanoparticles deposited on porous graphene surfaces for high performance of lithium ion batteries. *Nanoscale* **2012**, *4*, 5924–5930. [CrossRef] [PubMed]
38. Li, D.H.; Yang, D.J.; Zhu, X.Y.; Jing, D.W.; Xia, Y.Z.; Ji, Q.; Cai, R.S.; Li, H.L.; Che, Y.K. Simple pyrolysis of cobalt alginate fibres into Co_3O_4/C nano/microstructures for a high-performance lithium ion battery anode. *J. Mater. Chem. A* **2014**, *2*, 18761–18766. [CrossRef]
39. Du, H.R.; Huang, K.F.; Li, M.; Xia, Y.Y.; Sun, Y.X.; Yu, M.K.; Geng, B.Y. Gas template-assisted spray pyrolysis: A facile strategy to produce porous hollow Co_3O_4 with tunable porosity for high-performance lithium-ion battery anode materials. *Nano. Res.* **2018**, *11*, 1490–1499. [CrossRef]
40. Chen, D.M.; Wang, Z.; Wu, Y.C.; Feng, P.; Wang, W.J.; Huang, Z.Q.; Chen, J. Introducing heteroatoms, oxygen vacancies and heterostructures in Co_3O_4 wrapped in carbon nanofibers by low-temperature vulcanization for lithium-ion storage. *J. Alloys Compd.* **2024**, *970*, 172529. [CrossRef]
41. Adeniyi, A.G.; Iwuozor, K.O.; Emenike, E.C.; Sagboye, P.A.; Micheal, K.T.; Micheal, T.T.; Saliu, O.D.; James, R. Biomass-derived activated carbon monoliths: A review of production routes, performance, and commercialization potential. *J. Clean. Prod.* **2023**, *423*, 138711. [CrossRef]
42. Zhang, X.; Zhu, H.; Wei, Y.; Bao, J.; Zhang, N. Oxygen vacancies tuning over Co_3O_4 nanosheet preferentially growing (2 2 0) facet for efficient Hg^0 removal from flue gas. *Fuel* **2024**, *361*, 130675. [CrossRef]
43. Yue, F.; Duan, W.; Li, R.; Huang, M.; Wei, T.; Lv, X.; Wu, J.; Yang, C.; Yang, C.; Lu, Y.; et al. Ce dissolution induced in situ generating oxygen defects of Co_3O_4 boosting electrocatalytic oxidation of 5-hydroxymethylfurfural. *Appl. Surf. Sci.* **2024**, *649*, 159223. [CrossRef]
44. Li, Z.; Deng, L.; Kinloch, I.A.; Young, R.J. Raman spectroscopy of carbon materials and their composites: Graphene, nanotubes and fibres. *Prog. Mater. Sci.* **2023**, *135*, 101089. [CrossRef]
45. Kamali, A.R. *Green Production of Carbon Nanomaterials in Molten Salts and Applications*; Springer Nature: Singapore, 2023.
46. Kamali, A.R. Nanocatalytic conversion of CO_2 into nanodiamonds. *Carbon* **2017**, *123*, 205–215. [CrossRef]
47. Kamali, A.R.; Feighan, J.; Fray, D.J. Towards large scale preparation of graphene in molten salts and its use in the fabrication of highly toughened alumina ceramics. *Faraday Discuss.* **2016**, *190*, 451–470. [CrossRef] [PubMed]
48. Lu, X.; Lian, G.J.; Parker, J.; Ge, R.; Sadan, M.K.; Smith, R.; Cumming, D. Effect of carbon blacks on electrical conduction and conductive binder domain of next-generation lithium-ion batteries. *J. Power Sources* **2024**, *5921*, 233916. [CrossRef]
49. Senthilkumar, B.; Khan, Z.; Kim, S.P.K.; Ko, H.; Kim, Y. Highly porous graphitic carbon and $Ni_2P_2O_7$ for a high performance aqueous hybrid supercapacitor. *J. Mater. Chem. A* **2015**, *3*, 21553–21561. [CrossRef]
50. Thommes, M.; Kaneko, K.; Neimark, A.V.; Olivier, J.P.; Rodriguez-Reinoso, F.; Rouquerol, J.; Sing, K.S.W. Physisorption of gases, with special reference to the evaluation of surface area and pore size distribution (IUPAC Technical Report). *Pure Appl. Chem.* **2015**, *87*, 1051–1069. [CrossRef]

51. Wang, R.; Li, J.W.; Han, B.; Wang, Q.R.; Ke, R.H.; Zhang, T.; Ao, X.H.; Zhang, G.Z.; Liu, Z.B.; Qian, Y.X.; et al. Unique double-layer solid electrolyte interphase formed with fluorinated ether-based electrolytes for high-voltage lithium metal batteries. *J. Energy Chem.* **2024**, *88*, 532–542. [CrossRef]
52. Liu, W.; Placke, T.; Chau, K.T. Overview of batteries and battery management for electric vehicles. *Energy Rep.* **2022**, *8*, 4058–4084. [CrossRef]
53. Huang, Z.; Yang, H.E.Z.; Jiang, W.; Wang, Q.; Wang, S.; Ju, J.; Kwon, Y.U.; Zhao, Y. Improved capacity and cycling stability of SnO_2 nanoanode induced by amorphization during cycling for lithium-ion batteries. *Mater. Des.* **2019**, *180*, 107973. [CrossRef]
54. Amin, A.S.; Zhao, W.; Toloueinia, P.; Perera, I.P.; Fee, J.; Su, Y.; Posada, L.F.; Suib, S.L. Cycling-Induced Capacity Increase of Bulk and Artificially Layered $LiTaO_3$ Anodes in Lithium-Ion Batteries. *ACS Nano* **2023**, *17*, 20203–20217. [CrossRef]
55. AbdelHamid, A.A.; Mendoza-Garcia, A.; Lee, S.S.; Ying, J.Y. Metal oxide- and metal-loaded mesoporous carbon for practical high-performance Li-ion battery anodes. *Nano Energy* **2024**, *119*, 109025. [CrossRef]
56. Huang, G.Y.; Xu, S.M.; Lu, S.S.; Li, L.Y.; Sun, H.Y. Micro-/Nanostructured Co_3O_4 anode with enhanced rate capability for lithium-ion batteries. *ACS Appl. Mater. Interfaces* **2014**, *6*, 7236–7243. [CrossRef]
57. Xiong, C.Y.; Li, B.B.; Dang, W.H.; Zhao, W.; Duan, C.; Dai, L.; Ni, Y.H. Co/CoS nanofibers with flower-like structure immobilized in carbonated porous wood as bifunctional material for high-performance supercapacitors and catalysts. *Mater. Des.* **2020**, *195*, 108942. [CrossRef]
58. Wu, J.F.; Zuo, L.; Song, Y.H.; Chen, Y.Q.; Zhou, R.H.; Chen, S.H.; Wang, L. Preparation of biomass-derived hierarchically porous carbon/Co_3O_4 nanocomposites as anode materials for lithium-ion batteries. *J. Alloys Compd.* **2016**, *656*, 745–752. [CrossRef]
59. Zhuo, L.H.; Wu, Y.Q.; Ming, J.; Wang, L.Y.; Yu, Y.C.; Zhang, X.B.; Zhao, F.Y. Facile synthesis of a Co_3O_4-carbon nanotube composite and its superior performance as an anode material for Li-ion batteries. *J. Mater. Chem. A* **2013**, *1*, 1141–1147. [CrossRef]
60. Zhang, P.; Guo, Z.P.; Huang, Y.D.; Jia, D.Z.; Liu, H.K. Synthesis of Co_3O_4/carbon composite nanowires and their electrochemical properties. *J. Power Sources* **2011**, *196*, 6987–6991. [CrossRef]
61. Kim, H.; Seo, D.H.; Kim, S.W.; Kim, J.; Kang, K. Highly reversible Co_3O_4/graphene hybrid anode for lithium rechargeable batteries. *Carbon* **2011**, *49*, 326–332. [CrossRef]
62. Hou, Y.; Wang, Q.; Zhou, K.; Zhang, L.; Tan, T. Integrated machine learning methods with oversampling technique for regional suitability prediction of waste-to-energy incineration projects. *Waste Manag.* **2024**, *174*, 251–262. [CrossRef]
63. Taer, E.; Apriwandi, A.; Farma, R.; Taslim, R. Synthesis of highly self-N-O-dual doped unique carbon blooming flower-like nanofiber derived novel snake-plant waste for ultrahigh energy of solid-state-supercapacitor. *Chem. Eng. Sci.* **2024**, *285*, 119566. [CrossRef]
64. Kamali, A.R.; Zhao, H. Electrochemical conversion of natural graphite minerals into carbon nanostructures incorporated with Fe_3Si for Li-ion storage application. *J. Alloys Compd.* **2023**, *949*, 169819. [CrossRef]
65. Biber, B.; Sander, S.; Martin, J.; Wohlfahrt-Mehrens, M.; Mancini, M. Improved production process with new spheroidization machine with high efficiency and low energy consumption for rounding natural graphite for Li-ion battery applications. *Carbon* **2023**, *201*, 847–855. [CrossRef]
66. Ferdoush, M.R.; Al Aziz, R.; Karmaker, C.L.; Debnath, B.; Limon, M.H.; Bari, A. Unraveling the challenges of waste-to-energy transition in emerging economies: Implications for sustainability. *Innov. Green Dev.* **2024**, *3*, 100121. [CrossRef]
67. Boulanger, N.; Talyzin, A.V.; Xiong, S.; Hultberg, M.; Grimm, A. High surface area activated carbon prepared from wood-based spent mushroom substrate for supercapacitors and water treatment. *Colloids Surf. A* **2024**, *680*, 132684. [CrossRef]
68. Wei, S.; Kamali, A.R. Green conversion of waste PET into magnetic $Ni_{0.4}Fe_{2.6}O_4$/(Fe,Ni)@carbon nanostructure for adsorption and separation of dyes from aqueous media. *Chemosphere* **2023**, *342*, 140172. [CrossRef] [PubMed]
69. Radenković, M.; Petrović, J.; Pap, S.; Krstulović, N.; Živković, S. Waste biomass derived highly-porous carbon material for toxic metal removal: Optimisation, mechanisms and environmental implications. *Chemosphere* **2024**, *347*, 140684. [CrossRef]
70. Arıcı, Ş.; Kaçmaz, E.G.; Kamali, A.R.; Ege, D. Influence of graphene oxide and carbon nanotubes on physicochemical properties of bone cements. *Mater. Chem. Phys.* **2023**, *293*, 126961. [CrossRef]
71. Ege, D.; Nawaz, Q.; Beltrán, A.M.; Boccaccini, A.R. Effect of Boron-Doped Mesoporous Bioactive Glass Nanoparticles on C_2C1_2 Cell Viability and Differentiation: Potential for Muscle Tissue Application. *ACS Biomater. Sci. Eng.* **2022**, 5273–5283. [CrossRef]
72. Wang, S.; Chai, Y.; Wang, Y.; Luo, G.; An, S. Review on the Application and Development of Biochar in Ironmaking Production. *Metals* **2023**, *13*, 1844. [CrossRef]
73. DiGiovanni, C.; Li, D.; Ng, K.W.; Huang, X. Ranking of Injection Biochar for Slag Foaming Applications in Steelmaking. *Metals* **2023**, *13*, 1003. [CrossRef]
74. Meng, T.; Shi, H.; Ao, F.; Lu, Y.; Zhao, Y. Study on Nitrogen-Doped Biomass Carbon-Based Composite Cobalt Selenide Heterojunction and Its Electrocatalytic Performance. *Metals* **2023**, *13*, 767. [CrossRef]
75. Golroudbary, S.R.; Farfan, J.; Lohrmann, A.; Kraslawski, A. Environmental benefits of circular economy approach to use of cobalt. *Glob. Environ. Change* **2022**, *76*, 102568. [CrossRef]
76. Parekh, M.H.; Palanisamy, M.; Pol, V.G. Reserve lithium-ion batteries: Deciphering in situ lithiation of lithium-ion free vanadium pentoxide cathode with graphitic anode. *Carbon* **2023**, *203*, 561–570. [CrossRef]

77. Ln, X.; Xiong, X.; Cui, J.; Hu, R. Reducing voltage hysteresis of metal oxide anodes to achieve high energy efficiency for Li-ion batteries. *J. Energy Chem.* **2023**, *83*, 433–444. [CrossRef]
78. Zhou, S.; Meng, X.; Fu, C.; Chang, Z.; Chen, Y.; Xu, D.; Lin, S.; Han, C.; Chang, Z.; Pan, A. Lithiophilic Magnetic Host Facilitates Target-Deposited Lithium for Practical Lithium-Metal Batteries. *Small* **2023**, *19*, 2207764. [CrossRef]